A Preliminary Control Net of Mars[1]

MERTON E. DAVIES
The Rand Corporation, Santa Monica, California 90406

RICHARD A. BERG
Aeronautical Chart and Information Center, USAF
St. Louis, Missouri 63166

A control net for Mars has been computed from measurements of 112 points identified on the Mariner 6 and 7 pictures, and areocentric coordinates of these points are presented. The coordinates of an initial point are determined, and the near-encounter frames of Mariner 6 and the adjoining near-encounter frames of Mariner 7 are tied to this initial point; then the far-encounter pictures of Mariner 6 and 7 are joined to the near-encounter pictures. The near-encounter Mariner 7 polar pass is located without reference to the far-encounter frames.

This paper discusses progress to date on efforts to establish an areodetic control net of Mars from the Mariner 6 and 7 television pictures. Since this work is continuing, it is anticipated that improved results will be reported at a future time. Previous reports described the Mariners' missions, pictures, and television camera characteristics [*Leighton et al.*, 1969*a*, *b*, *c*].

When this effort started there was little experience in making precise measurements on television pictures and only little more experience in the reduction of small-scale pictures to establish a control net. TV pictures have had limited usefulness because they contain very large geometric distortions and only a few picture elements (pixels) per picture. However, careful preflight calibration of the Mariner vidicon tubes permitted eventual removal of most of the geometrical deformations [*Rindfleisch et al.*, 1971]. The Mariner pictures contained $704 \times 935 = 6.6 \times 10^5$ pixels; for comparison, a typical high-quality conventional 9 in. $\times$ 9 in. photograph from an aerial mapping camera might contain approximately $(9 \times 25 \times 40)^2 = 8.1 \times 10^7$ pixels. Thus it is necessary to take many vidicon pictures (more than 123 in the example above) to cover the same surface area at the same pixel size as might be taken by one aerial picture. Errors associated with tying many pictures together through photogrammetric techniques are cumulative; hence there is considerable advantage to using high-resolution large-format pictures, as is standard mapping practice.

An initial planet-wide control system [*Berg*, 1970] was computed as accurate trajectory data became available, and control-point measurements were made as soon as geometrically restored pictures were obtained. This initial net was completed in time to use it for control in some early mapping projects. (This initial control net is being used by the U.S. Army Topographic Command for their new 1 : 25,000,000 scale chart of Mars.) The preliminary control net reported in this paper is an update of the earlier network and incorporates a new comprehensive measurement program. Additional improvements are planned for the future.

This report first considers the analytic data-reduction method and equations, thus defining the input needs. Then the Mariner trajectory information and picture characteristics are discussed. The control points are next defined and the picture measurements presented. Finally the results of the computations and the control-net coordinates are given.

ANALYTIC DATA REDUCTION

Clearly identifiable marks (control points) on the surface of Mars are selected from the pictures. Most frequently the control points

[1] Contribution RM-6381-JPL of the Rand Corporation.

TABLE 1. The Trajectory Parameters

Picture Frame	UT Hr	UT Min	UT Sec	*RS*, km	*RX*	*RY*	*RZ*
6N5	−0	11	10.272	8516.75	−0.76743601	0.64076662	−0.02144871
6N7	−0	9	45.786	8149.34	−0.80827934	0.58863917	−0.01372568
6N9	−0	8	21.300	7816.89	−0.84868851	0.52886698	−0.00524189
6N11	−0	6	56.814	7524.24	−0.88740114	0.46098088	0.00397782
6N13	−0	5	32.328	7276.40	−0.92286577	0.38487243	0.01385480
6N15	−0	4	7.842	7078.27	−0.95333070	0.30095299	0.02424534
6N17	−0	2	43.356	6934.30	−0.97701675	0.21027978	0.03493779
6N19	−0	1	18.871	6848.02	−0.99236245	0.11459346	0.04566281
6N21	0	0	5.615	6821.70	−0.99829238	0.01621328	0.05611974
6N23	0	1	30.101	6856.06	−0.99442576	−0.08221589	0.06601463
7N5	−0	17	35.777	10426.97	−0.53684159	0.75787418	−0.37071254
7N7	−0	16	11.298	9962.54	−0.56721053	0.72883654	−0.38349638
7N9	−0	14	46.816	9516.08	−0.59923105	0.69540421	−0.39665490
7N11	−0	13	22.333	9090.43	−0.63272946	0.65691437	−0.41002061
7N13	−0	11	57.851	8688.81	−0.66739636	0.61266402	−0.42334955
7N15	−0	10	32.335	8310.51	−0.70318203	0.56128268	−0.43645934
7N17	−0	9	8.886	7972.79	−0.73808060	0.50412071	−0.44844098
7N19	−0	7	44.404	7666.96	−0.77244418	0.43870877	−0.45919992
7N23	−0	4	55.439	7182.92	−0.83325867	0.28478582	−0.47389558
7N25	−0	3	30.954	7013.92	−0.85679937	0.19730736	−0.47640804
7N27	−0	2	6.474	6898.92	−0.87383027	0.10451194	−0.47486616
6F39	−16	26	15.212	429267.19	0.10710523	0.98838578	−0.10780523
6F40	−15	22	53.641	401840.03	0.10590856	0.98852073	−0.10775014
6F41	−15	21	29.155	401230.50	0.10588013	0.98852393	−0.10774883
6F42	−14	25	9.942	376848.18	0.10466612	0.98865932	−0.10769273
6F43	−13	28	50.698	352463.75	0.10328386	0.98881167	−0.10762862
6F44	−12	32	31.431	328074.96	0.10169558	0.98898432	−0.10755466
6F45	−11	37	36.623	304293.30	0.09990147	0.98917627	−0.10747074
6F46	−10	41	17.312	279897.66	0.09774399	0.98940281	−0.10736935
6F47	−9	44	57.980	255497.50	0.09517390	0.98966651	−0.10724786
6F48	−8	48	38.630	231092.01	0.09205996	0.98997705	−0.10709969
6F49	−7	52	19.265	206680.05	0.08820905	0.99034756	−0.10691502
7F62	−30	48	34.671	787290.67	0.10158776	0.99306245	−0.05921885
7F63	−30	13	23.208	772355.75	0.10142400	0.99307387	−0.05930778
7F64	−29	36	47.245	756821.20	0.10124662	0.99308623	−0.05940397
7F65	−29	0	11.268	741287.27	0.10106186	0.99309905	−0.05950417
7F66	−28	24	59.721	726350.57	0.10087670	0.99311186	−0.05960455
7F67	−27	48	23.695	710816.19	0.10067569	0.99312572	−0.05971339
7F69	−20	54	30.287	535132.49	0.09758534	0.99333242	−0.06138212
7F70	−20	6	38.247	514811.81	0.09709114	0.99336436	−0.06164835
7F71	−19	20	10.652	495086.98	0.09657253	0.99339755	−0.06192762
7F72	−18	32	18.559	474763.70	0.09599299	0.99343422	−0.06223957
7F73	−17	45	50.913	455037.06	0.09538085	0.99347249	−0.06256890
7F74	−16	59	23.248	435308.95	0.09471308	0.99351370	−0.06292805
7F75	−16	11	31.086	414982.44	0.09395842	0.99355958	−0.06333371
7F76	−15	25	3.375	395250.61	0.09315144	0.99360782	−0.06376729
7F77	−14	37	11.171	374919.91	0.09223118	0.99366183	−0.06426161
7F80	−12	16	23.394	315111.38	0.08883412	0.99385174	−0.06608446
7F81	−11	29	55.594	295369.65	0.08741065	0.99392692	−0.06684767
7F82	−10	43	27.781	275625.13	0.08578269	0.99400972	−0.06771997
7F83	−9	55	35.472	255278.79	0.08384176	0.99410395	−0.06875949
7F85	−8	21	15.298	215172.53	0.07893981	0.99432043	−0.07138187
7F86	−7	34	47.435	195411.63	0.07578433	0.99444344	−0.07306799
7F87	−6	48	19.561	175645.07	0.07191717	0.99457680	−0.07513225
7F88	−6	0	27.196	155272.83	0.06690097	0.99472125	−0.07780661
7F93	−5	1	18.970	130095.28	0.05852987	0.99489060	−0.08226124

Data from *Campbell et al.* [1970].

TABLE 2. The Control Points and Where They Are Found

Point Number	Location	Reference Frames
1	Center of bright ring	7F70, 7F71, 7F72, 7F73, 7F74, 7F75, 7F76, 7F77
2	Center of crater	6N23, 6F49
3	Center of crater	6N23, 6F49
4	Center of crater	6F39, 6F40, 6F41, 6F42 6F43, 6F44, 6F45, 6F46, 7F80, 7F81, 7F82, 7F83, 7F85
5	Center of crater	6N19, 6N21, 7N9
6	Center of crater	6N9, 6N11, 7N5, 7N7
7	Center of crater	6N9, 6N11
8	Center of crater	6N9, 6N11
9	Center of crater	6N19, 6N21, 7N9
10	Center of crater	6N9, 6N11, 7N5, 7N7
11	Center of crater	6N9, 6N11, 7N5, 7N7
12	Center of crater	6N21, 7N9
13	Center of crater	6N21, 7N9
14	Center of crater	6N13, 6N19
15	Center of crater	6N7, 6N15
16	Center of crater	6N7, 6N15
17	Center of crater	7N9, 7N23
18	Center of crater	6N15, 6N17
19	Center of crater	6N15, 6N17
20	Center of crater	6N15, 6N17
21	Center of crater	6N7, 6N15
22	Center of crater	6N7, 6N15, 6N17
23	Center of crater	7N9, 7N23
24	Center of crater	7N9, 7N23
25	Center of light spot	7N11, 7N13
26	Center of crater	6N17, 6N18, 6N19
27	Center of crater	6N17, 6N19
28	Center of crater	6N17, 6N19
29	Center of crater	6N17, 6N19
30	Center of crater	6N17, 6N19
31	Center of crater	6N11, 6N13, 7N5, 7N7, 7N9
32	Center of crater	6N13, 7N5, 7N7, 7N9
33	Center of crater	6N11, 6N13, 7N5, 7N7
34	Center of crater	6N11, 6N13, 7N5, 7N7, 7N9
35	Center of crater	6N11, 6N13, 7N5, 7N7, 7N9
36	Center of crater	7N25, 7N27
37	Center of crater	6N11, 6N13
38	Center of crater	6N11, 6N13, 7N5, 7N7, 7N9
39	Center of crater	6N11, 6N19
40	Center of light spot	7N11, 7N13, 7N15
41	Center of light spot	7N11, 7N13, 7N15
42	Center of light spot	7N11, 7N13
43	Center of dark spot	7N11, 7N13, 7N15
44	Center of dark spot	7N11, 7N13, 7N15
45	Center of light spot	7N13, 7N15
46	Center of light spot	7N13, 7N15
47	Center of crater	7N17, 7N19
48	Center of light spot in crater	7N15, 7N17
49	Center of crater	7N15, 7N17
50	End of dark strip	6N5, 7F69, 7F70, 7F71
51	Center of dark spot	6N5, 7F69, 7F70, 7F71
52	Center of dark spot	6N5, 7F69, 7F70, 7F71
53	Center of crater	7N15, 7N17
54	Center of crater	7N13, 7N15, 7N17
55	Center of crater	7N13, 7N15, 7N17
56	Center of crater	6N19, 6N20, 6N21
57	Center of dark spot	7N13, 7N15, 7N17
58	Center of crater	6N19, 6N21
59	Center of crater	6N19, 6N21
60	Center of crater	6N19, 6N21
61	Center of crater	6N19, 6N21
62	Center of crater	6N21, 6N22, 6N23
63	Center of crater	6N21, 6N23

TABLE 2. *(continued)*

Point Number	Location	Reference Frames
64	Center of crater	6N21, 6N23
65	Center of crater	6N21, 6N23
66	Center of crater	7N15, 7N17, 7N19
67	Center of dark spot	7N15, 7N17, 7N19
68	Center of light spot	7N15, 7N17, 7N19
69	Center of crater	7N19, 7N23
70	Center of crater	7N17, 7N19
71	Center of crater	7N17, 7N19
72	Center of crater	7N13, 7N15
73	Center of light tip	7F69, 7F70, 7F71, 7F72, 7F73, 7F74, 7F75
74	Center of dark spot	7F69, 7F70, 7F71, 7F72, 7F73, 7F74, 7F75, 7F76
75	Center of dark spot	7F69, 7F70, 7F71, 7F72, 7F73
76	Center of light spot	7F70, 7F71, 7F72, 7F73, 7F74, 7F75, 7F76, 7F77
77	Center of dark spot	6F39, 6F40, 6F41, 6F42, 6F43
78	Center of light tip	7F3, 7F74, 7F75, 7F76, 7F77
79	Center of crater	6N13, 7N7, 7N9, 6F49, 7F65, 7F66, 7F67
80	Center of crater	7N25, 7N27
81	Center of dark tip	7F77, 7F80, 7F81, 7F82, 7F83
82	Center of dark spot	7F81, 7F82, 7F83, 7F85, 7F86, 7F87
83	Center of light spot	6F39, 6F40, 6F41, 6F42, 6F43, 7F77, 7F80, 7F81, 7F82, 7F83, 7F85
84	Center of dark spot	6F46, 6F47, 6F48, 6F49, 7F62, 7F63, 7F64, 7F65, 7F66, 7F67, 7F88, 7F93
85	Center of dark spot	6F44, 6F45, 6F46, 6F47, 6F48, 7F62, 7F63, 7F64, 7F65, 7F66, 7F67, 7F86, 7F87
86	Center of crater	6F46, 6F47, 6F48, 6F49, 7F86, 7F87, 7F88
87	Center of dark spot	6F42, 6F43, 6F44, 6F45, 7F80, 7F81, 7F82, 7F83, 7F85, 7F86, 7F87
88	Center of crater	7N25, 7N27
89	Center of crater	7N25, 7N27
90	Center of dark spot	6F47, 6F48, 6F49
91	Center of crater	7N25, 7N27
92	Center of dark spot	6F40, 6F41, 6F42, 6F43, 6F44, 7F80, 7F81, 7F82, 7F83
93	Center of light spot	6F39, 6F40, 6F41, 6F42, 6F43, 6F44, 6F45, 6F46, 7F62, 7F63
94	Center of light tip	6F42, 6F43, 6F44, 6F45, 6F46, 6F47
95	Center of crater	6F45, 6F46, 6F47
96	Center of light tip	6F39, 6F40, 6F41, 6F42, 6F43
97	Center of dark spot	6F39, 6F40, 6F41, 6F42, 6F43
98	Center of crater	7N23, 7N25
99	Center of crater	7N23, 7N25
100	Center of crater	7N23, 7N25
101	Center of crater	7N23, 7N25
102	Center of crater	7N23, 7N25
103	Center of crater	7N13, 7N15, 7F69, 7F70, 7F71
104	Center of crater	7F69

TABLE 2. (*continued*)

Point Number	Location	Reference Frames
105	Center of dark spot	7F86, 7F87, 7F88, 7F93
106	Center of crater	6N5, 6N7
107	Center of crater	6N5, 6N7
108	Center of light spot	6N5, 6N7
109	Center of light spot	6N5, 6N7
110	Center of crater	6N13, 6N21
111	Center of crater	6N13, 6N21
112	Center of crater	6N5, 6N7

are centers of craters; sometimes they are particularly dark or light markings on the planet. To be useful they must be found on at least two and preferably many more pictures. The coordinates of the control points are measured in pixels (x, y), and in using calibration data these are referred to the vidicon face in millimeters (x_0, y_0). Estimates of the areocentric coordinates (radius R, latitude φ, and longitude λ) of these control points are made, and, with knowledge of the time of picture taking and the spacecraft position on the trajectory, vidicon coordinates (x_c, y_c) of the control points can be computed using the camera focal length. Improved areocentric coodinates are determined in a manner that minimizes the weighted sum of the squares of the differences between the measured points x_0, y_0 and the computed points x_c, y_c.

The geometric equations relating a Mars-fixed surface point to its position in the image plane of a camera aboard a moving spacecraft are

$$\begin{vmatrix}\xi\\ \eta\\ \zeta\end{vmatrix} = [C] \times \left\{[m]^T \times [V]^T \times \begin{vmatrix}R\cos\varphi\cos(360^\circ - \lambda)\\ R\cos\varphi\sin(360^\circ - \lambda)\\ R\sin\varphi\end{vmatrix} - \begin{vmatrix}S_x\\ S_y\\ S_z\end{vmatrix}\right\} \qquad (1)$$

$$x_c = \frac{\xi}{\zeta} f, \qquad y_c = \frac{\eta}{\zeta} f$$

where x_c, y_c are the computed vidicon coordinates of the control points referred to the principal point. The parameters in equation 1 are as follows:

R, φ, λ = areocentric radius (in km), latitude, and longitude of a surface point.

$[V]^T$ = 3×3 orthogonal matrix to remove diurnal rotation, rotating an areocentric vector from the *fixed* Mars-equatorial coordinate system to the *inertial* Mars-equatorial coordinate system.

$[m]^T$ = 3×3 orthogonal matrix, rotating an areocentric vector from the inertial Mars-equatorial coordinate system to the 1950.0 earth-ecliptic coordinate system.

S_x, S_y, S_z = areocentric 1950.0 earth-ecliptic coordinates of the spacecraft (in km).

$[C]$ = 3×3 orthogonal matrix rotating a camera-centered vector from the 1950.0 earth-ecliptic coordinate system to the camera-fixed coordinate system.

ξ, η, ζ = camera-centered camera-fixed coordinates of a Martian surface point (in km).

f = camera focal length (in mm).

x_c, y_c = coordinates of a Martian surface point in vidicon coordinates (in mm).

To determine corrections to inaccurately known parameters it is necessary to establish a system of observational equations of the form [*Arthur*, 1965]

$$\begin{aligned}(x_0 - x_c)_{i,j} &= \frac{\partial x_{c,i}}{\partial R_i}\Delta R_i + \frac{\partial x_{c,i}}{\partial \varphi_i}\Delta\varphi_i + \frac{\partial x_{c,i}}{\partial \lambda_i}\Delta\lambda_i + \cdots = \sum_{k=1}^{n}\frac{\partial x_{c,i}}{\partial P_k}\Delta P_k\\ (y_0 - y_c)_{i,j} &= \frac{\partial y_{c,i}}{\partial R_i}\Delta R_i + \frac{\partial y_{c,i}}{\partial \varphi_i}\Delta\varphi_i + \frac{\partial y_{c,i}}{\partial \lambda_i}\Delta\lambda_i + \cdots = \sum_{k=1}^{n}\frac{\partial y_{c,i}}{\partial P_k}\Delta P_k\end{aligned} \qquad (2)$$

in which point i is measured $(x_0, y_0)_{i,j}$ on picture j and P_k is any parameter. Thus there are two equations for each point measured on each picture. Corrections to the parameters ΔP_k are determined by minimizing $(x_0 - x_c)_{i,j}$ and $(y_0 - y_c)_{i,j}$ by least squares. Thus improved estimates of the parameters P_k are obtained in successive iterations if the number of observation equations exceeds the number of variables.

Equations 1 and 2 are general and can be used to solve for each control point's coordinates R, φ, λ, the spacecraft positions S_x, S_y, S_z and camera-pointing matrix $[C]$ at each shutter time, and the planet's spin-axis matrix $[m]$. Of course, care must be taken to observe correlations between these various parameters because it is frequently not possible to improve the values of all variables independently.

The computation of the partial derivatives can be made directly or by an approximation in which $x_{c_i} + \delta x_{c_i}$ results from a change of one of the parameters, say, R_i to $R_i + \delta R_i$ [*Arthur*, 1965]. In this case,

$$(\partial x_{c,i}/\partial R_i) \sim (\delta x_{c,i}/\delta R_i)$$

Computation of the partial derivatives is a time-consuming task however it is done. The rotation matrices $[C]$ and $[m]$ can be improved by solving independently for a correction along each axis. As an example, $\Delta\alpha$ (the correction to the camera yaw axis) [*Arthur*, 1968] can be found from the observation equation in which

$$(\partial x_{c,i}/\partial \alpha) \sim (\delta x_{c,i}/\delta \alpha)$$

and $x_{c,i} + \delta x_{c,i}$ results from changing the $[C]$ matrix to

$$[C] \begin{vmatrix} 1 & 0 & 0 \\ 0 & 1 & \delta\alpha \\ 0 & -\delta\alpha & 1 \end{vmatrix}$$

Since $\delta\alpha$ is small, $\cos \delta\alpha \sim 1$ and $\sin \delta\alpha \sim \delta\alpha$. In this manner all three axes of the $[C]$ matrix can be considered variables, as can the two axes of the $[m]$ matrix that define the planet's spin axis.

The observational equations are accumulated to form a normal matrix in double precision. Matrix inversion is carried out in double precision arithmetic to control numerical roundoff

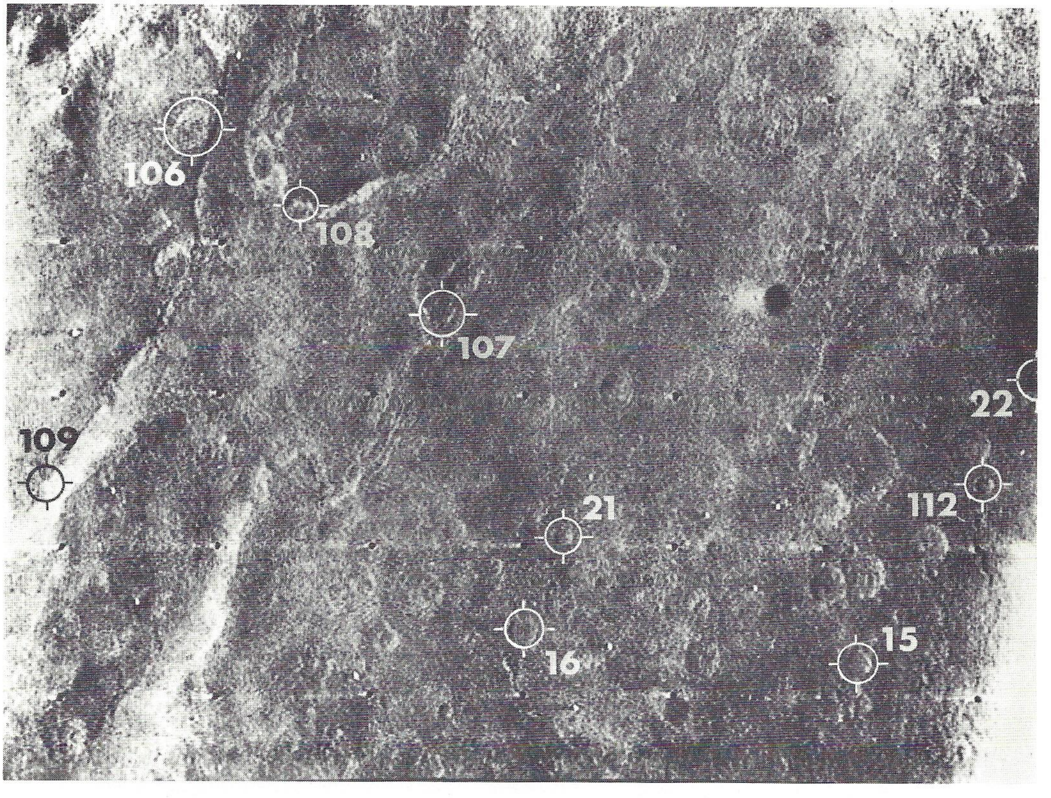

Fig. 1. Frame 6N7 with locations of points 15, 16, 21, 22, 106, 107, 108, 109, and 112 identified.

errors often associated with inversions of large matrices. The standard errors of the parameters are the square roots of the diagonals of the inverted normal matrix, and parameter corrections ΔP_k are found by matrix multiplication of the inverted normal matrix with the right-hand side.

In summary, to obtain a least-squares solution of the observation equations, the number of equations must exceed the number of variables. Measurements (x_0, y_0) of the same control point are made on two or more pictures, and the total number of equations is twice (one x and one y) the total number of points measured on each picture. The variables can be the radius, latitude, and longitude (R, φ, λ) of each control point, the spacecraft position (S_x, S_y, S_z), and the camera-pointing matrix ($[C]$) of each picture, and the planet-spin axis ($[m]$).

Trajectory Parameters

The Mariner 6 and 7 flyby trajectories and their camera-pointing strategy have been reported previously [*Leighton et al.*, 1969*c*]. The position of the spacecraft relative to Mars and the camera-aiming direction at the time the pictures were taken are determined from the trajectory computations, the position of the scan platform, and the telemetry reports of the spacecraft attitude within the limit cycle of the startracker [*Campbell*, 1970]. This analysis is the source of many of the input parameters required for solution of equation 1; the spacecraft position in areocentric 1950.0 earth-ecliptic coordinates (S_x, S_y, S_z) and the time of picture taking are given. Table 1 gives values of these parameters for those pictures used in the analysis.

The matrix

$$[V]^T = \begin{bmatrix} \cos V & -\sin V & 0 \\ \sin V & \cos V & 0 \\ 0 & 0 & 1 \end{bmatrix}$$

is defined by the hour angle of the Mars vernal

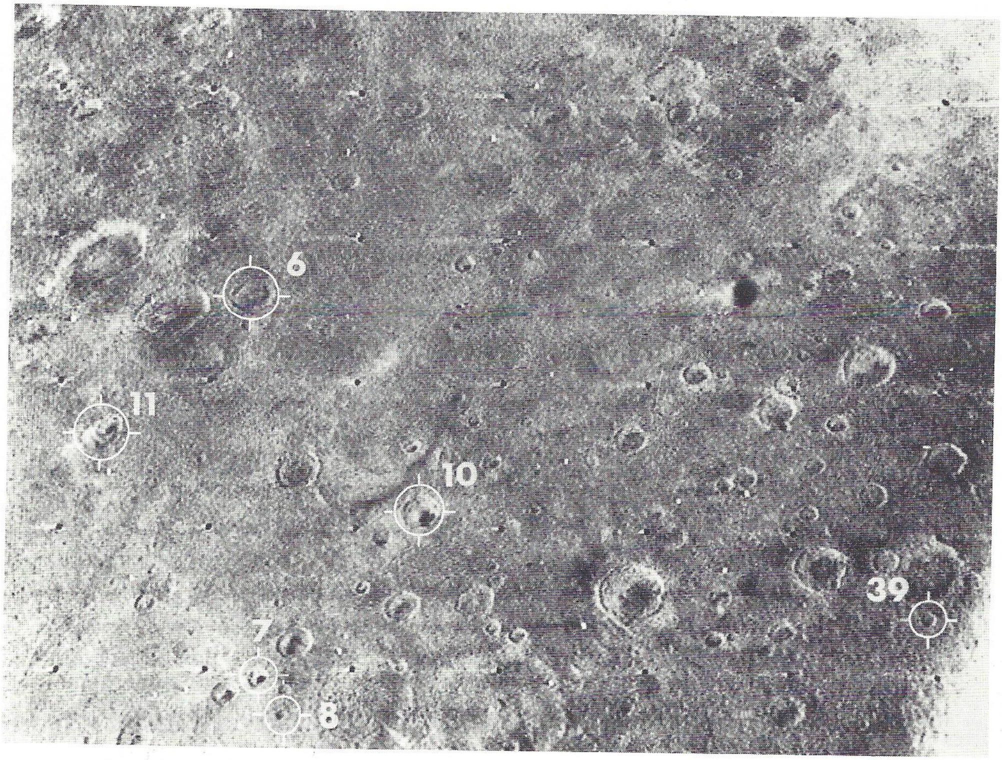

Fig. 2. Frame 6N11 with locations of points 6, 7, 8, 10, 11, and 39 identified.

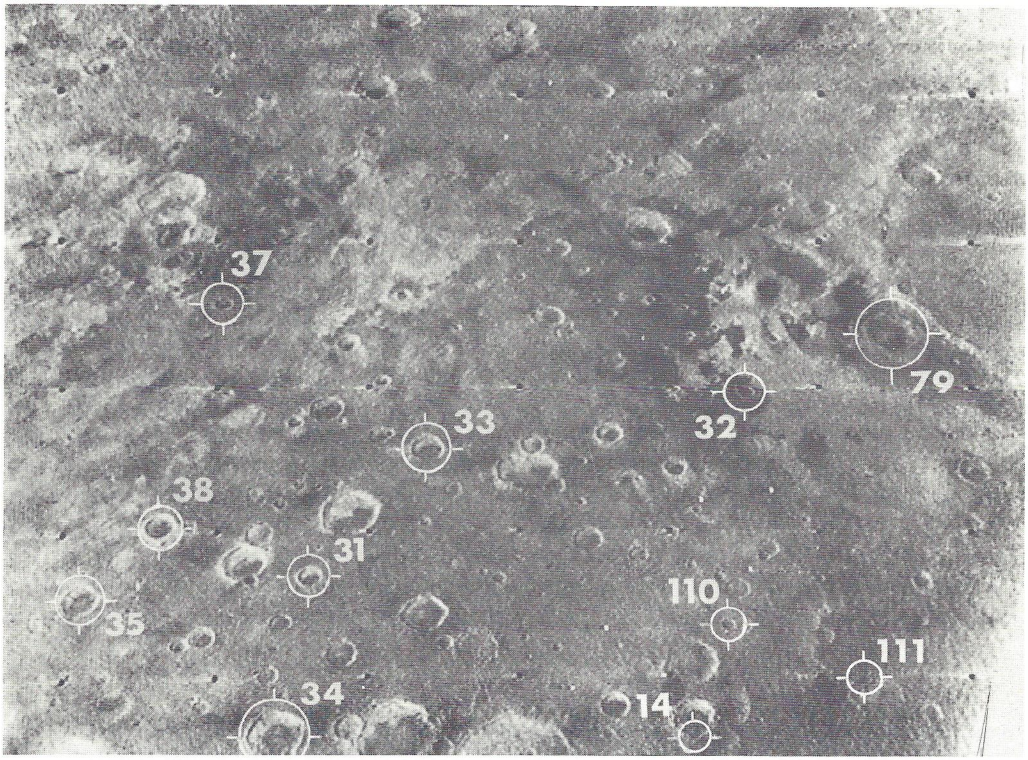

Fig. 3. Frame 6N13 with locations of points 14, 31, 32, 33, 34, 35, 37, 38, 79, 110, and 111 identified.

equinox V, which is given by

$$V = 149°.475 + 350.891962(\text{JD} - 2418322.0) \quad \text{Mod } 360°$$

where JD is the Julian ephemeris date. The time that pictures were taken (UT) in Table 1 is given relative to the Julian date of closest approach (JDCA). Thus

$$\text{JD} = \text{JDCA} + \text{UT}$$

where

JDCA = 2440433.7216 (Mariner 6).
JDCA = 2440438.7089 (Mariner 7).

The matrix $[m]$ relates the Mars-fixed coordinate system to the 1950.0 ecliptic coordinate system at the time of the Mariner flybys and is given by [*Campbell*, 1970].

where m_3 is in the direction of the Mars spin axis, and m_1 is in the direction of the prime meridian in 1950.0 ecliptic coordinates.

The spacecraft coordinates (S_x, S_y, S_z) are determined from the tabulated distances from the center of Mars to the spacecraft, RS, and the direction cosines (RX, RY, RZ) of the Mars-to-spacecraft vector in 1950.0 ecliptic coordinates.

CAMERA FOCAL LENGTHS AND PICTURE SCALE

The focal lengths of the television camera lenses were determined from preflight calibration measurements [*Adams et al.*, 1970] in which a target was placed in the focal plane of the collimator and angular measurements (φ_i) of its size were made with a theodolite. The image size (r_i) was then measured in the focal plane

$$[m]^T = \begin{bmatrix} -0.09811451 & 0.89311749 & 0.43899282 \\ -0.99500078 & -0.07978033 & -0.06007115 \\ -0.01862760 & -0.44269205 & 0.89648020 \end{bmatrix}$$

of the lens with a traveling micrometer microscope.

If a radial lens distortion function (δ_i) of the form [*Brown*, 1956]

$$\delta_i = K_3 r_i^3 + K_5 r_i^5 + \cdots$$

is assumed, then the measurement residuals (d_i) will be

$$d_i = f \tan \varphi_i - r_i - K_3 r_i^3 - K_5 r_i^5 - \cdots$$

for any value of the focal length (f). The preferred values of f, together with the distortion constants K_3, K_5, $K \cdots$ are determined by minimizing the sum of the squares of the residuals (Σd_i^2). The estimated errors of measurements (r_i) are 2 μ for the Mariner B camera lenses, 10 μ for the Mariner 6A camera lens, and 5 μ for the Mariner 7A camera lens. Since the distortions of these lenses were small compared with these measurement errors, K_3, K_5, $\cdots$ were assumed to be zero. The focal lengths then are

Camera Lens	Focal Length f, mm	Standard Error d_i, μ
M6A	51.96	3.8
M6B	505.44	1.7
M7A	52.60	2.7
M7B	502.66	2.3

The measurements of the control points were made on GEOM 3 pictures that had been processed by a machine program designed to remove the optical and electronic distortions so that the positional data are geometrically correct [*Rindfleisch et al.*, 1971]. The format of GEOM 3 pictures is approximately 950 × 750 pixels. The coordinates of the control points are measured in pixels from the upper left-hand corner of the picture, using specially prepared pictures that have a pixel grid superimposed to facilitate counting. The origin is then translated to the central reseau point, which corresponds approximately to the intersection of the lens' principal axis with the vidicon surface.

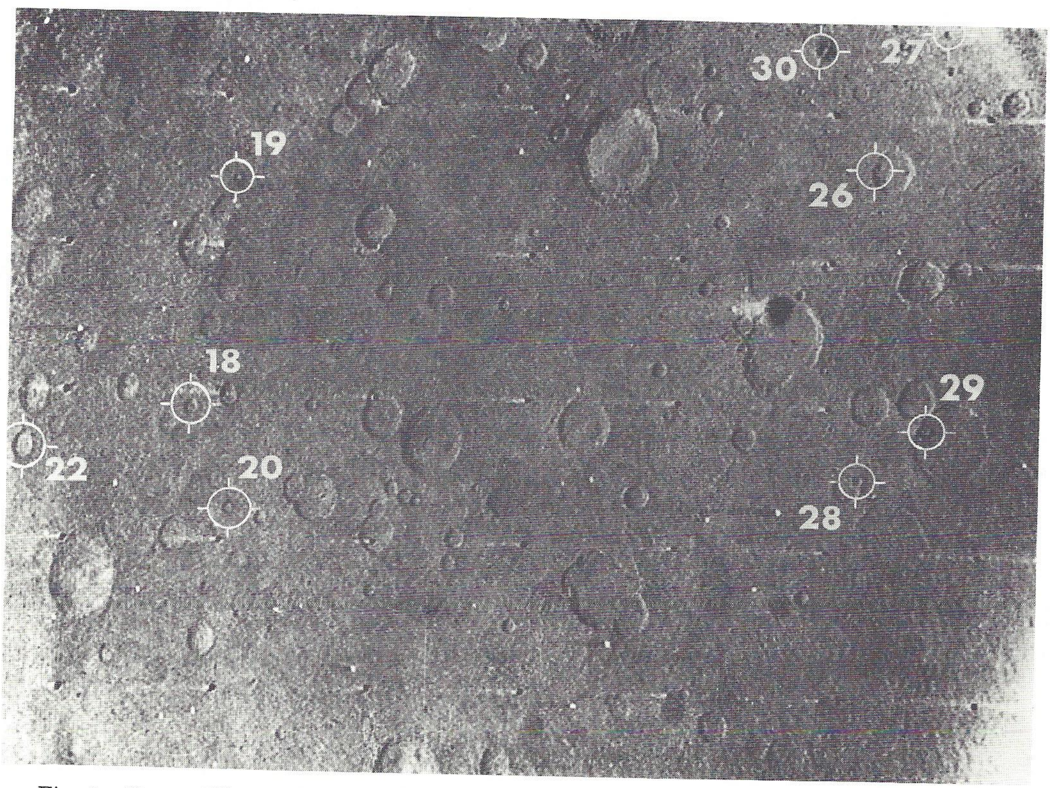

Fig. 4. Frame 6N17 with locations of points 18, 19, 20, 22, 26, 27, 28, 29, and 30 identified.

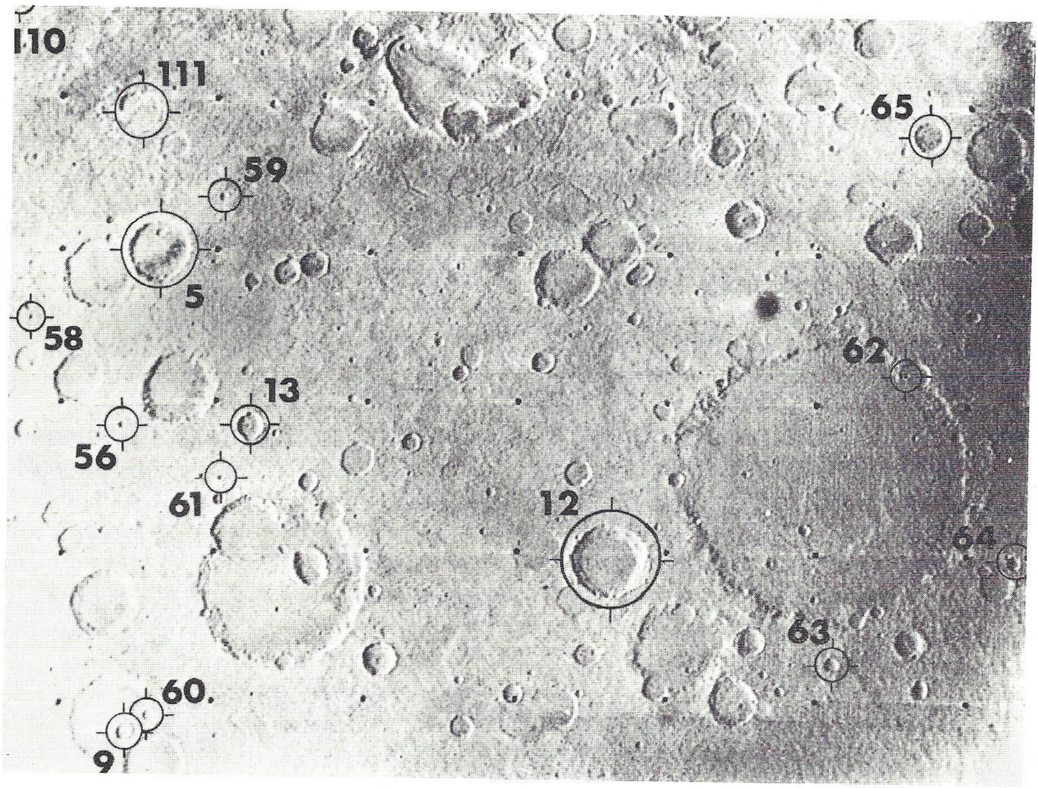

Fig. 5. Frame 6N21 with locations of points 5, 9, 12, 13, 56, 58, 59, 60, 61, 62, 63, 64, 65, 110, and 111 identified.

Since GEOM 3 pictures are essentially free from distortions, it is only necessary to determine the size of a pixel as measured on the vidicon surface to transform pixel counts to vidicon coordinates. The size of the pixel was determined by a least-squares fit of the coordinates of the 35 reseau points in GEOM 3 pixel coordinates to the preflight measurements of the reseau point locations on the vidicon face. Results of this computation of the GEOM 3 pixel size, the standard error, and the pixel coordinates of the central reseau point are

Camera	Pixel Coordinates of the Central Reseau Point		Size of GEOM 3 Pixel, mm	Standard Error, μ
M6A	512	387	0.013276	15.4
M6B	516	387	0.013486	8.5
M7A	514	387	0.013546	14.3
M7B	514	387	0.013650	8.1

The vidicon coordinates of a point are then determined from the pixel coordinates by

M6A
$$x_0 = 0.013276(512 - x)$$
$$y_0 = 0.013276(387 - y)$$

M6B
$$x_0 = 0.013486(516 - x)$$
$$y_0 = 0.013486(387 - y)$$

M7A
$$x_0 = 0.013546(514 - x)$$
$$y_0 = 0.013546(387 - y)$$

M7B
$$x_0 = 0.013650(514 - x)$$
$$y_0 = 0.013650(387 - y)$$

CONTROL POINTS

Control points have been selected from most of the Mariner 6 and 7 pictures and are listed in Table 2, together with those frames on which they can be found. Crater centers are the most common control points because there are many of them (in the near-encounter pictures) and they are easy to identify and measure. In the

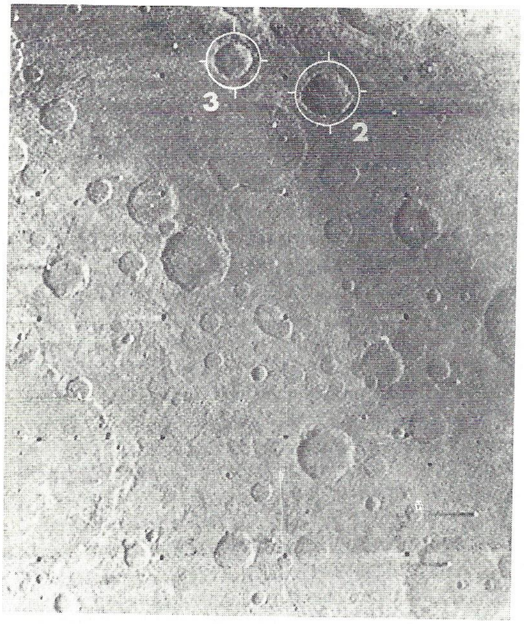

Fig. 6. Frame 6N23 with locations of points 2 and 3 identified.

south polar region, certain dark or light spots were used, as they are small and distinctive. In the far-encounter pictures, craters are usually difficult to identify on successive frames because of the flat lighting and the poor resolution. Consequently a number of albedo points (light and dark spots) are used in those areas when necessary. The problem in choosing the light spots (which are easy to identify) is that they may be atmospheric effects and not lie on the surface. The Mariner 6 near-encounter points are identified on Figures 1–6, and the Mariner 7 identification points on Figures 7–10. All the far-encounter control points can be seen on Figure 11.

The Mariner 6 near-encounter pictures all have overlapping areas so they can be readily tied together. One strip of Mariner 7 near-encounter pictures overlaps the Mariner 6 pictures, so that they are easily joined. Since the polar strip (of Mariner 7) does not join any other near-encounter pictures, they must be tied to far-encounter pictures, which in turn are

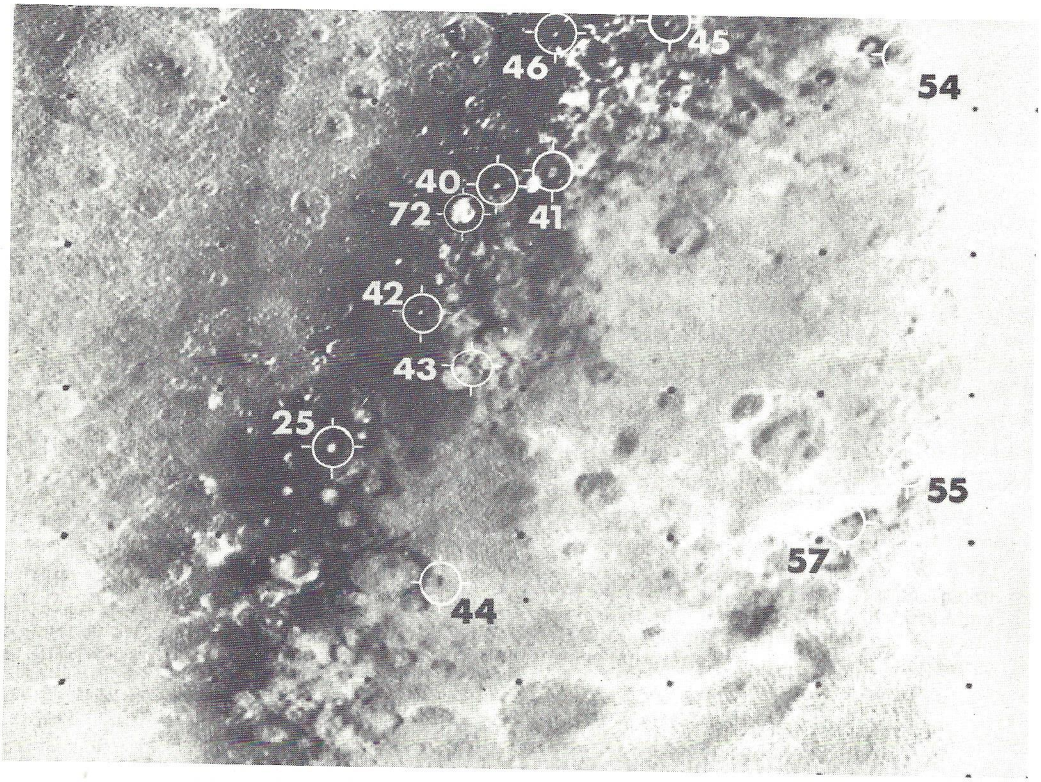

Fig. 7. Frame 7N13 with locations of points 25, 40, 41, 42, 43, 44, 45, 46, 54, 55, 57, and 72 identified.

Fig. 8. Frame 7N17 with locations of points 47, 48, 49, 53, 54, 55, 66, 67, 68, 70, and 71 identified.

tied to the Mariner 6 near-encounter. Because it is important to tie all sequences and strips together into just one control system, those points that are common to both near-encounter and far-encounter pictures are of special importance.

Perhaps the most interesting point is 79 because it is found on near-encounter frames of Mariner 6 (6N13) and Mariner 7 (7N7, 7N9) as well as on far-encounter pictures (6N49, 7F65, 7F66, 7F67) of both missions. Points 2 and 3 are found on both near-encounter (6N23) and far-encounter (6F49). This is also true of points 50, 51, and 52 (6N5, 7F69, 7F70, 7F71). So far, it is not possible to tie the polar strip to far-encounter with confidence as the quality of the far-encounter pictures are so poor.

The Measurements

All measurements of the control points were made on GEOM 3 pictures by counting pixels (picture elements) from the upper left-hand corner of the frame. To aid in counting, specially prepared pictures were formed in which a dark and light dash is superimposed on each twenty-fifth row and column to form a reference grid. Pixel counting is laborious at best; however, it is probably the most accurate method to measure television pictures.

A few experiments were made in an effort to devise procedures to help make precise measurements and to select control points that can be precisely measured. The aim was to achieve a repeatability of better than one pixel: hopefully, one-tenth of a pixel. The measurements were made on large prints (16 × 20), in which the single pixel was easily seen. Templets were made by scribing circles of various sizes on a piece of acetate with dividers. To measure the center of a crater, a circle was superimposed on top of the circular or elliptical lip of the crater, and the coordinates in pixels of the center of the acetate circle could be read directly. With this method, it is easy to read the coordinates to one-tenth of a pixel, but frequently the crater's rim was badly enough defined to lead to considerable variation in repeated measurements.

The plane was to make at least three measurements of each point and in most cases that was done; a few had just two when a gross error was thrown out, many had four, and some that were used for experimentation had ten or more. The arithmetic means of the point measurements were used in the calculations and are listed together with the vidicon coordinates (x_0, y_0) in Table 3 for the Mariner 6 near-encounter pictures, Table 4 for the Mariner 7 near-encounter pictures, Table 5 for the Mariner 6 far-encounter pictures, and Table 6 for the Mariner 7 far-encounter pictures. The rms of the point measurements was calculated and was less than one pixel deviation for more than half of the points. The rms exceeded two pixels on only a few points in the far-encounter sequences.

RESULTS

A few computer runs of the differential improvement procedure were first made to test the accuracy of the basic data and to decide which parameters to assume as known and which to treat as unknowns. All computations to date have assumed that the spacecraft positions (S_x, S_y, S_z) as given are correct. Except for a few tests no adjustment of the areocentric radius (R_i) to surface points is made; the assumed equatorial radius is 3393.4 km with an adopted polar flattening of 21 km.

Because the Mariner 6 trajectory is known with more accuracy than that of Mariner 7, a set of Mariner 6 pictures (near- and far-encounter) were chosen to attempt to improve the current estimate [*de Vaucouleurs*, 1964] of Mars spin axis. Test computer runs were made assuming the camera-pointing matrix [C] was accurate; other tests permitted improvement of the roll angle, and still others treated all three

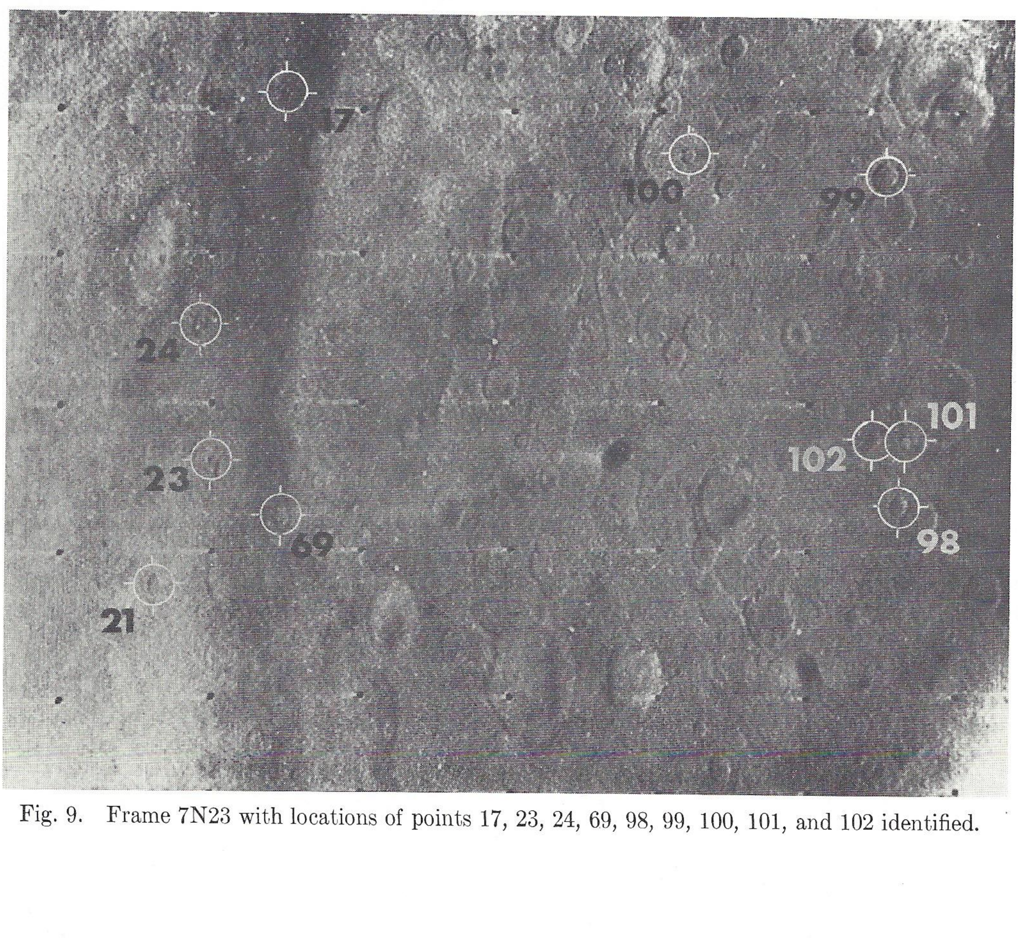

Fig. 9. Frame 7N23 with locations of points 17, 23, 24, 69, 98, 99, 100, 101, and 102 identified.

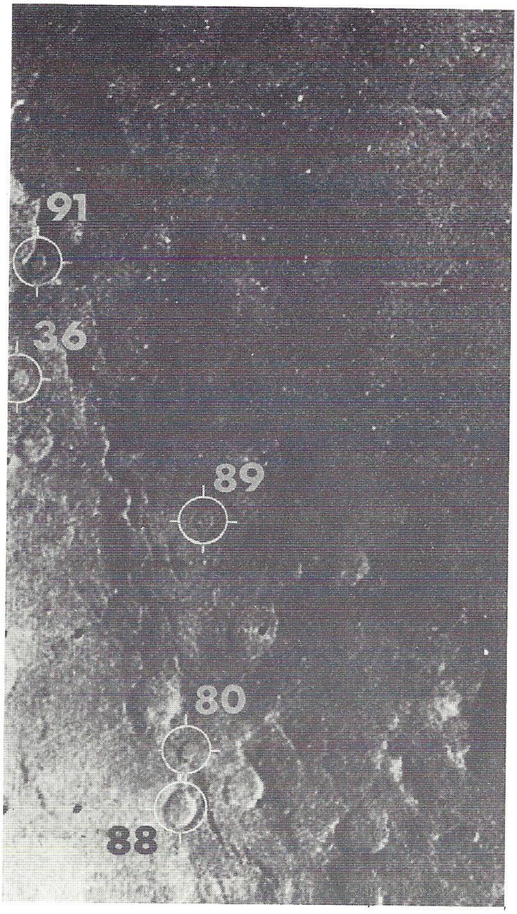

Fig. 10. Frame 7N27 with locations of points 36, 80, 88, 89, and 91 identified.

axes as variables. In most cases, the standard error of the spin-axis corrections was larger than the indicated corrections themselves, hence it is not possible to infer an improvement. Consequently in the solution for the planet-wide control net no improvement in the spin axis was sought.

The method used in determining the coordinates of the 112 points of the control net consists of defining an initial point (62) and solving for its coordinates. Then the points on the Mariner 6 near-encounter pictures and frames 7N5, 7N7, 7N9, 7N23, 7N25, 7N27 from Mariner 7 near encounter are tied to the initial point. The far-encounter sequences have points in common with the near-encounter sequences, and they therefore can be added to the net. Finally, the Mariner 7 polar pass (frames 7N11, 7N13, 7N15, 7N17, 7N19) is located without reference to the far-encounter frames. In these computations, improvements are sought in the areocentric coordinates of the points and the three axes of the camera-pointing matrix [C]. Weighting factors, inversely proportional to the square of the combined standard errors of measurement and GEOM 3 calibration, have been used in the computations. Table 7 lists the areocentric latitudes, longitudes, and standard errors of the points in the control net. Except for the polar pass, the standard errors are internal and refer to the error with respect to point 62.

Since the absolute accuracy of the net depends

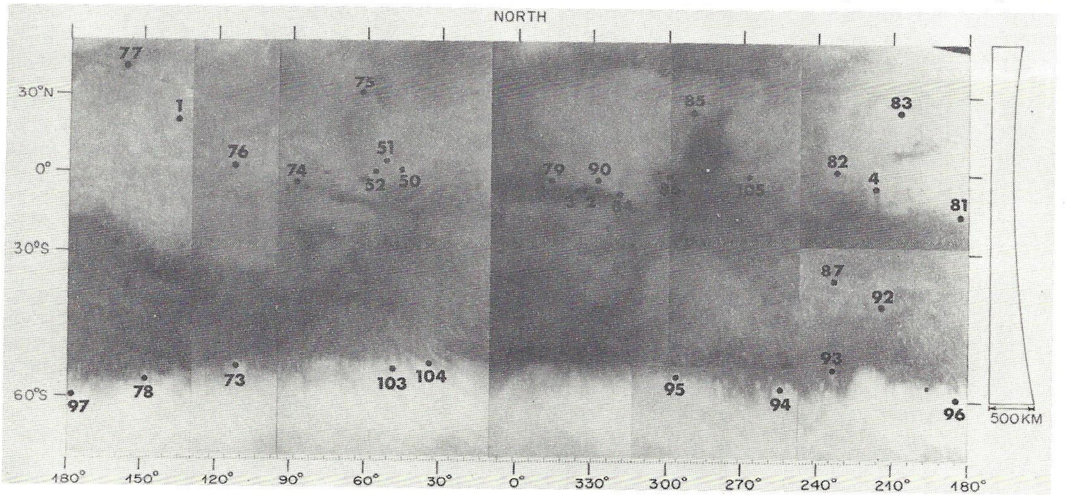

Fig. 11. Mercator photomap with locations of points 1, 2, 3, 4, 50, 51, 52, 73, 74, 75, 76, 77, 78, 79, 81, 82, 83, 84, 85, 86, 87, 90, 92, 93, 94, 95, 96, 97, 103, 104, and 105 identified.

TABLE 3. Control Point Measurements, Mariner 6 Near Encounter

Point	GEOM 3 Pixel Coordinates (mean) ⟨x⟩	⟨y⟩	Vidicon Coordinates, mm x_0	y_0
		Picture 6N5		
50	653.0	586.1	−1.8719	−2.6428
51	829.4	518.3	−4.2138	−1.7436
52	883.4	255.2	−4.9307	1.7498
106	373.9	679.0	1.8339	−3.8770
107	141.5	524.8	4.9188	−1.8294
108	277.0	614.2	3.1194	−3.0163
109	487.8	388.0	0.3219	−0.0133
		Picture 6N7		
15	214.6	140.1	3.9489	3.2776
16	526.3	176.0	−0.1898	2.8019
21	477.7	257.6	0.4554	1.7179
22	55.4	394.1	6.0621	−0.0940
106	806.5	629.8	−3.9095	−3.2231
107	587.3	460.8	−0.9997	−0.9791
108	715.5	561.2	−2.7017	−2.3120
109	937.0	313.1	−5.6423	0.9811
112	105.2	303.4	5.4013	1.1105
		Picture 6N9		
6	289.8	555.2	2.9499	−2.2325
7	249.0	222.9	3.4913	2.1786
8	226.3	189.6	3.7927	2.6212
10	117.0	367.0	5.2437	0.2659
11	396.5	442.9	1.5334	−0.7418
		Picture 6N11		
6	746.8	469.3	−3.1172	−1.0926
7	738.4	110.9	−3.0052	3.6655
8	719.7	75.3	−2.7572	4.1379
10	590.2	266.2	−1.0379	1.6037
11	878.5	346.5	−4.8657	0.5381
31	201.8	347.8	4.1178	0.5211
33	110.9	456.0	5.3254	−0.9158
34	217.7	212.2	3.9075	2.3210
35	393.6	332.6	1.5719	0.7218
37	299.0	584.9	2.8284	−2.6268
38	332.8	394.9	2.3795	−0.1044
39	117.4	164.6	5.2392	2.9532
		Picture 6N13		
14	361.5	54.0	1.9980	4.4209
31	703.0	211.5	−2.5362	2.3304
32	308.0	377.8	2.7083	0.1221
33	596.6	327.2	−1.1231	0.7935
34	734.6	64.8	−2.9550	4.2775
35	908.2	194.3	−5.2593	2.5581
37	776.4	467.9	−3.5095	−1.0740
38	836.7	261.7	−4.3102	1.6630
79	173.2	432.2	4.4983	−0.6005
110	327.4	160.1	2.4507	3.0123
111	202.0	95.2	4.1151	3.8744
		Picture 6N15		
15	497.0	146.0	0.1989	3.1870
16	712.3	228.5	−2.6585	2.1042
18	167.8	451.5	4.5700	−0.8563

TABLE 3. (*continued*)

Point	GEOM 3 Pixel Coordinates (mean) ⟨x⟩	⟨y⟩	Vidicon Coordinates, mm x_0	y_0
19	131.6	665.1	5.0502	−3.6926
20	128.9	357.5	5.0858	0.3912
21	673.5	307.6	−2.1434	1.0548
22	334.7	412.5	2.3542	−0.3389
112	391.2	314.0	1.6037	0.9691
		Picture 6N17		
18	811.3	377.1	−3.9735	0.1314
19	772.6	588.9	−3.4597	−2.6804
20	778.2	282.5	−3.5341	1.3873
22	956.7	339.8	−5.9036	0.6273
26	202.7	603.7	4.1063	−2.8769
27	139.0	728.0	4.9519	−4.5271
28	215.8	314.7	3.9324	0.9599
29	155.4	362.6	4.7342	0.3239
30	254.1	712.0	3.4239	−4.3147
		Picture 6N19		
5	121.3	618.4	5.1876	−3.0714
9	135.9	179.9	4.9938	2.7495
26	873.7	374.2	−4.8019	0.1699
27	812.4	497.9	−3.9881	−1.4723
28	895.3	89.3	−5.0887	3.9523
29	840.5	134.8	−4.3607	3.3480
30	913.0	480.6	−5.3232	−1.2423
14	347.0	729.0	2.1905	−4.5404
39	631.7	726.8	−1.5895	−4.5114
56	149.3	461.1	4.8152	−0.9838
58	237.8	558.4	3.6403	−2.2755
59	63.4	668.2	5.9556	−3.7332
60	112.4	194.8	5.3051	2.5516
61	54.9	412.5	6.0685	−0.3385
		Picture 6N21		
5	833.3	526.3	−4.2651	−1.8493
9	867.8	92.3	−4.7240	3.9129
12	430.4	242.1	1.0833	1.9241
13	753.0	367.0	−3.1991	0.2655
14	171.4	533.7	4.5218	−1.9476
56	867.1	369.9	−4.7143	0.2270
58	945.5	466.6	−5.7551	−1.0568
59	775.6	575.6	−3.4996	−2.5039
60	845.3	106.7	−4.4249	3.7213
61	780.3	321.1	−3.5620	0.8749
62	160.4	408.9	4.6678	−0.2907
63	229.6	143.8	3.7491	3.2287
64	64.7	237.1	5.9384	1.9901
65	138.4	626.6	4.9599	−3.1809
110	954.3	751.2	−5.8715	−4.8356
111	859.5	658.3	−4.6139	−3.6013
		Picture 6N23		
2	598.8	637.5	−1.1524	−3.3250
3	701.6	677.9	−2.5165	−3.8620
62	885.3	313.5	−4.9559	0.9758
63	963.6	50.6	−5.9954	4.4660
64	800.8	142.5	−3.8341	3.2460
65	852.6	528.8	−4.5218	−1.8825

TABLE 4. Control Point Measurements, Mariner 7 Near Encounter

Point	GEOM 3 Pixel Coordinates (mean) ⟨x⟩	⟨y⟩	Vidicon Coordinates, mm x_0	y_0
	Picture 7N5			
6	548.8	261.4	−0.717	1.7021
10	437.5	247.9	1.0359	1.8846
11	526.0	157.1	−0.1626	3.1138
31	388.4	451.8	1.7014	−0.8771
32	360.8	694.6	2.0749	−4.1664
33	410.2	538.8	1.6061	−2.0559
34	335.9	393.5	2.9122	−0.0884
35	424.9	356.7	1.2066	0.4108
38	435.0	409.4	1.0708	−0.3038
	Picture 7N7			
6	787.5	151.8	−3.7048	3.1867
10	680.1	134.5	−2.2500	3.6210
11	761.6	43.5	−3.3543	4.6534
31	630.4	344.4	−1.5761	0.5767
32	599.8	596.4	−1.1619	−2.8362
33	649.4	436.4	−1.8741	−0.6687
34	582.0	282.5	−0.9216	1.4151
35	667.2	248.8	−2.0752	1.8724
38	677.4	300.9	−2.2127	1.1666
79	580.8	685.8	−0.9049	−4.0475
	Picture 7N9			
5	689.2	434.0	−2.3728	−0.6362
9	516.0	364.7	−0.0275	0.3025
12	498.5	602.4	0.2104	−2.9178
13	613.1	459.2	−1.3424	0.9780
14	598.7	699.4	−1.1469	−4.2318
17	253.0	682.3	3.5351	−4.0006
21	284.5	328.0	3.1084	0.7988
23	235.6	433.1	3.7717	−0.6245
24	287.3	513.8	3.0704	−1.7176
31	906.9	230.5	−5.3222	2.1199
32	876.8	490.0	−4.9145	−1.3952
34	863.4	161.3	−4.7332	3.0571
35	946.5	128.6	−5.8586	3.5003
38	953.2	185.0	−5.9499	2.7363
69	139.5	423.8	5.0730	−0.4980
79	853.4	587.6	−4.5999	−2.7178
	Picture 7N11			
25	361.0	412.3	2.0730	−0.3423
40	212.7	645.0	4.0814	−3.4944
41	165.8	658.2	4.7172	−3.6741
42	280.6	532.7	3.1621	−1.9732
43	241.9	484.3	3.6859	−1.3180
44	281.2	296.5	3.1535	1.2264
	Picture 7N13			
25	682.9	332.0	−2.2875	0.7455
40	540.5	576.5	−0.3585	−2.5674
41	491.0	589.8	0.3111	−2.7471
42	606.3	458.6	−1.2507	−0.9694
43	561.7	407.9	−0.6461	−0.2836
44	587.2	212.6	−0.9916	2.3624

TABLE 4. *(continued)*

Point	GEOM 3 Pixel Coordinates (mean) ⟨x⟩	⟨y⟩	Vidicon Coordinates, mm x_0	y_0
45	390.9	727.3	1.6680	−4.6097
46	490.0	715.6	0.3251	−4.4517
54	183.0	703.2	4.4837	−4.2837
55	173.9	325.2	4.6065	0.8371
57	226.8	270.9	3.8904	1.5731
72	569.3	552.3	−0.7491	−2.2392
	Picture 7N15			
40	910.4	500.0	−5.3696	−1.5311
41	857.6	514.5	−4.6540	−1.7271
43	919.9	323.2	−5.4979	0.8642
44	929.5	117.3	−5.6284	3.6538
45	757.6	658.2	−3.2998	−3.6741
46	863.7	648.6	−4.7366	−3.5436
48	535.5	727.2	−0.2908	−4.6083
49	289.0	312.0	3.0483	1.0164
53	387.0	502.9	1.7203	−1.5700
54	530.9	632.5	−0.2285	−3.3251
55	489.4	236.2	0.3332	2.0432
57	545.8	180.8	−0.4308	2.7927
66	167.0	315.6	4.7005	0.9676
67	150.8	539.3	4.9199	−2.0631
68	162.4	458.0	4.7623	−0.9618
72	939.6	473.6	−5.7652	−1.1731
	Picture 7N17			
47	144.0	578.3	5.0116	−2.5913
48	942.2	638.6	−5.8004	−3.4082
49	640.1	203.3	−1.7086	2.4879
53	764.5	402.1	−3.3933	−0.2045
54	931.4	537.8	−5.6536	−2.0423
55	857.4	122.8	−4.6512	3.5784
57	911.7	63.7	−5.3872	4.3801
66	504.7	206.1	0.1267	2.4511
67	504.5	439.0	0.1287	−0.7037
68	511.1	354.6	0.0400	0.4389
70	386.7	461.9	1.7244	−1.0139
71	230.0	545.4	3.8471	−2.1450
	Picture 7N19			
47	520.5	470.0	−0.0874	−1.1243
66	903.8	74.5	−5.2802	4.2338
67	919.3	319.6	−5.4895	0.9137
68	923.0	229.7	−5.5403	2.1308
70	790.0	344.3	−3.7380	0.5784
71	617.3	435.0	−1.3986	−0.6502
	Picture 7N23			
17	717.1	666.2	−2.7516	−3.7816
21	830.4	223.5	−4.2864	2.2143
23	778.9	333.9	−3.5883	0.7188
24	790.5	459.7	−3.7459	−0.9843
69	718.1	283.3	−2.7643	1.4052
98	168.6	295.9	4.6788	1.2337
99	183.6	594.7	4.4763	−2.8132
100	358.5	612.2	2.1061	−3.0499
101	163.1	354.9	4.7537	0.4344
102	192.9	357.3	4.3501	0.4019

TABLE 4. (continued)

Point	GEOM 3 Pixel Coordinates (mean) $\langle x \rangle$	$\langle y \rangle$	Vidicon Coordinates, mm x_0	y_0
	Picture 7N25			
36	341.9	627.1	2.3317	−3.2519
80	192.5	348.2	4.3546	0.5256
88	197.5	306.3	4.2873	1.0927
89	188.8	527.6	4.4056	−1.9050
91	331.0	715.7	2.4785	−4.4526
98	758.7	126.7	−3.3147	3.5256
99	765.4	422.8	−3.4055	−0.4845
100	916.4	447.6	−5.4514	−0.8213
101	751.1	184.2	−3.2122	2.7471
102	779.1	186.2	−3.5906	2.7200
	Picture 7N27			
36	958.4	444.6	−6.0195	−0.7802
80	833.6	162.6	−4.3290	3.0397
88	838.0	119.7	−4.3886	3.6215
89	824.0	339.0	−4.1996	0.6509
91	946.3	533.8	−5.8553	−1.9886

TABLE 5. Control Point Measurements, Mariner 6 Far Encounter

Point	GEOM 3 Pixel Coordinates (mean) $\langle x \rangle$	$\langle y \rangle$	Vidicon Coordinates, mm x_0	y_0
	Picture 6F39			
4	351.0	346.1	2.2080	0.5547
77	524.5	127.9	−0.1146	3.4942
83	387.4	195.0	1.7343	2.5893
93	407.9	588.6	1.4574	−2.7188
96	523.1	573.3	−0.0953	−2.5129
97	540.2	573.8	−0.3268	−2.5196
	Picture 6F40			
4	392.8	341.7	1.6618	0.6116
77	558.2	116.9	−0.5684	3.6432
83	427.5	182.0	1.1931	2.7646
92	443.5	549.3	0.9773	−2.1883
93	403.5	603.7	1.5172	−2.9220
96	530.5	597.8	−0.1955	−2.8422
97	545.6	595.7	−0.3987	−2.8150
	Picture 6F41			
4	397.0	340.8	1.6045	0.6231
77	562.1	113.6	−0.6217	3.6871
83	431.2	178.6	1.1443	2.8105
92	446.4	551.3	0.9386	−2.2157
93	407.7	605.8	1.4610	−2.9503
96	533.3	596.2	−0.2329	−2.8208
97	550.1	595.9	−0.4599	−2.8172
	Picture 6F42			
4	470.0	320.9	0.6204	0.8918
77	615.1	90.2	−1.3360	3.9968
83	500.2	150.7	0.2131	3.1867
87	417.5	524.2	1.3288	−1.8507

TABLE 5. (continued)

Point	GEOM 3 Pixel Coordinates (mean) $\langle x \rangle$	$\langle y \rangle$	Vidicon Coordinates, mm x_0	y_0
92	499.7	547.5	0.2203	−2.1645
93	438.5	605.8	1.0456	−2.9507
94	389.0	625.7	1.7127	−3.2196
96	567.9	598.3	−0.6999	−2.8500
97	586.3	598.6	−0.9485	−2.8541
	Picture 6F43			
4	552.7	318.1	−0.4949	0.9294
77	663.8	79.9	−1.9937	4.1411
83	578.0	144.1	−0.8357	3.2762
87	472.1	533.7	0.5925	−1.9784
92	554.8	562.6	−0.5237	−2.3686
93	475.0	625.1	0.5529	−3.2106
94	415.1	641.4	1.3603	−3.4313
96	602.9	624.3	−1.1719	−3.2007
97	618.1	622.8	−1.3769	−3.1793
	Picture 6F44			
4	637.9	298.0	−1.6441	1.2009
85	184.3	177.5	4.4740	2.8253
87	544.9	531.0	−0.3897	−1.9415
92	618.1	564.7	−1.3762	−2.3965
93	524.9	631.0	−0.1196	−3.2910
94	454.8	647.7	0.8260	−3.5158
	Picture 6F45			
4	747.6	297.9	−3.1235	1.2014
85	250.7	153.1	3.5774	3.1539
87	640.7	547.0	−1.6828	−2.1575
93	592.7	655.7	−1.0348	−3.6241
94	517.2	672.5	−0.0162	−3.8503
95	387.5	683.6	1.7325	−4.0008
	Picture 6F46			
4	830.2	281.5	−4.2373	1.4233
84	166.6	385.1	4.7120	0.0256
85	321.7	98.1	2.6210	3.8968
86	274.5	298.2	3.2572	1.2070
93	635.5	664.9	−1.6075	−3.7478
94	560.7	679.6	−0.6028	−3.9465
95	417.8	687.2	1.3243	−4.0485
	Picture 6F47			
84	213.2	360.2	4.0836	0.3611
85	399.8	56.1	1.5675	4.4625
86	350.4	272.3	2.2336	1.5475
90	130.1	319.7	5.2038	0.9076
94	591.3	707.3	−1.0148	−4.3189
95	420.8	706.5	1.4464	−4.3007
	Picture 6F48			
84	292.1	361.3	3.0200	0.3461
85	473.2	47.9	0.5779	4.5731
86	452.2	262.1	0.8611	1.6847
90	196.6	309.3	4.3074	1.0474
	Picture 6F49			
2	208.4	336.7	4.1483	0.6783
3	189.6	333.3	4.4018	0.7242
79	78.1	292.2	5.9055	1.2785
84	369.2	322.1	1.9797	0.8757
86	551.5	211.8	−0.4781	2.3634
90	261.0	265.0	3.4394	1.6453

TABLE 6. Control Point Measurements, Mariner 7 Far Encounter

Point	GEOM 3 Pixel Coordinates (mean) ⟨x⟩	⟨y⟩	Vidicon Coordinates, mm x_0	y_0
		Picture 7F62		
84	452.0	461.0	0.8463	−1.0104
85	498.3	355.6	0.2143	0.4283
93	578.3	548.8	−0.8777	−2.2086
		Picture 7F63		
84	507.2	443.9	0.0934	−0.7772
85	553.1	339.8	−0.5332	0.6443
93	624.1	540.3	−1.5022	−2.0925
		Picture 7F64		
84	478.8	437.2	0.4799	−0.6847
85	525.7	329.4	−0.1597	0.7862
		Picture 7F65		
79	465.1	433.3	0.6670	−0.6324
84	545.7	431.6	−0.4324	−0.6082
85	587.5	324.5	−1.0030	0.8529
		Picture 7F66		
79	495.2	444.9	0.2573	−0.7897
84	580.1	442.2	−0.9026	−0.7535
85	617.9	335.9	−1.4185	0.6981
		Picture 7F67		
79	496.1	428.3	0.2443	−0.5637
84	579.5	426.5	−0.8946	−0.5397
85	615.9	322.6	−1.3907	0.8791
		Picture 7F69		
50	674.3	380.3	−2.1876	0.0910
51	649.7	375.2	−1.8528	0.1606
52	632.9	402.1	−1.6225	−0.2061
73	574.1	624.8	−0.8207	−3.2460
74	514.2	443.4	−0.0033	−0.7699
75	576.7	288.4	−0.8562	1.3462
103	644.1	610.6	−1.7762	−3.0521
104	667.0	599.6	−2.0878	−2.9023
		Picture 7F70		
1	296.5	377.7	2.9689	0.1269
50	635.9	372.2	−1.6644	0.2020
51	612.5	365.6	−1.3450	0.2917
52	600.4	390.3	−1.1789	−0.0446
73	522.6	626.3	−0.1174	−3.2664
74	483.0	431.0	0.4234	−0.6006
75	536.6	275.7	−0.3078	1.5199
76	357.1	434.2	2.1420	−0.6443
103	589.2	611.1	−1.0268	−3.0583
		Picture 7F71		
1	346.5	353.4	2.2869	0.4581
50	693.7	357.8	−2.4525	0.3986
51	671.1	346.8	−2.1444	0.5483
52	662.1	371.6	−2.0216	0.2102
73	565.2	618.0	−0.6985	−3.1532
74	550.3	408.9	−0.4952	−0.2987

TABLE 6. (*continued*)

Point	GEOM 3 Pixel Coordinates (mean) ⟨x⟩	⟨y⟩	Vidicon Coordinates, mm x_0	y_0
75	596.3	252.6	−1.1227	1.8346
76	417.2	412.8	1.3213	−0.3518
103	638.5	605.2	−1.6987	−2.9781
		Picture 7F72		
1	424.3	347.0	1.2244	0.5465
73	628.3	631.0	−1.5597	−3.3311
74	640.1	406.8	−1.7215	−0.2703
75	667.7	247.4	−2.0983	1.9052
76	505.3	406.9	0.1184	−0.2710
		Picture 7F73		
1	423.9	334.9	1.2299	0.7112
73	609.7	640.1	−1.3060	−3.4545
74	644.4	401.4	−1.7800	−0.1971
75	656.3	241.4	−1.9417	1.9871
76	512.6	397.4	0.0188	−0.1416
78	477.8	668.8	0.4938	−3.8459
		Picture 7F74		
1	518.1	315.9	−0.0554	0.9705
73	679.5	642.9	−2.2584	−3.4930
74	736.7	389.7	−3.0402	−0.0372
76	610.6	381.8	−1.3182	0.0713
78	548.5	669.1	−0.4706	−3.8507
		Picture 7F75		
1	491.4	290.3	0.3082	1.3205
73	621.9	644.5	−1.4728	−3.5145
74	700.4	377.3	−2.5447	0.1324
76	588.6	360.9	−1.0186	0.3559
78	495.4	668.2	0.2546	−3.8384
		Picture 7F76		
1	552.5	273.2	−0.5258	1.5539
74	741.4	376.0	−3.1037	0.1508
76	648.5	350.7	−1.8352	0.4952
78	528.2	673.1	−0.1931	−3.9049
		Picture 7F77		
1	659.1	267.2	−1.9806	1.6356
76	755.5	351.1	−3.2965	0.4907
78	620.2	692.1	−1.4493	−4.1646
81	439.2	507.8	1.0217	−1.6482
83	267.4	327.4	3.3658	0.8133
		Picture 7F80		
4	350.7	453.8	2.2285	−0.9115
81	606.8	462.7	−1.2660	−1.0333
83	375.4	247.2	1.8916	1.9077
87	351.4	692.4	2.2200	−4.1693
92	454.5	707.2	0.8122	−4.3703
		Picture 7F81		
4	391.3	439.2	1.6754	−0.7123
81	654.6	445.9	−1.9185	−0.8033
82	268.6	417.1	3.3497	−0.4102
83	411.9	218.2	1.3942	2.3038

TABLE 6. *(continued)*

Point	GEOM 3 Pixel Coordinates (mean) $\langle x \rangle$	$\langle y \rangle$	Vidicon Coordinates, mm x_0	y_0
87	370.4	694.4	1.9604	−4.1955
92	473.9	708.9	0.5478	−4.3944
		Picture 7F82		
4	537.0	410.6	−0.3140	−0.3224
81	795.7	431.2	−3.8445	−0.6026
82	406.2	380.6	1.4715	0.0877
83	551.5	177.3	−0.5113	2.8621
87	486.8	686.9	0.3718	−4.0936
92	601.8	705.8	2.266	−1.1985
		Picture 7F83		
4	640.5	387.0	−1.7262	0.0003
81	887.1	421.1	−5.0928	−0.4655
82	501.5	356.2	0.1713	0.4204
83	644.0	137.7	−1.7748	3.4036
87	566.9	685.0	−0.7218	−4.0680
92	681.2	709.0	−2.2826	−4.3958
		Picture 7F85		
4	762.3	342.0	−3.3886	0.6139
82	620.1	291.2	−1.4479	1.3084
83	730.1	60.7	−2.9500	4.4534
87	649.7	699.6	−1.8518	−4.2675
		Picture 7F86		
82	873.0	249.1	−4.9000	1.8830
85	243.7	141.2	3.6901	3.3552
86	200.2	426.9	4.2834	−0.5440
87	875.1	701.8	−4.9290	−4.2963
105	550.1	400.5	−0.4923	−0.1838
		Picture 7F87		
82	935.0	212.5	−5.7467	2.3816
85	260.9	71.2	3.4551	4.3107
86	216.2	387.0	4.0650	−0.0005
87	916.1	708.0	−5.4880	−4.3817
105	611.5	364.9	−1.3313	0.3017
		Picture 7F88		
84	129.6	501.6	5.2476	−1.5637
86	334.0	347.3	2.4565	0.5424
105	781.5	320.6	−3.6509	0.9064
		Picture 7F93		
84	174.8	436.4	4.6304	−0.6749
105	934.5	260.3	−5.7398	1.7295

on the precision with which the initial point is located, it is desirable to select this point so as to minimize errors in its position on the Martian surface. It has been estimated that the standard error of the position of the Mariner 6 spacecraft is about 2 km and the error of the camera-pointing direction is about 0.2° in each coordinate. This angular error will translate into a minimum surface error when the distance along the optical axis is minimum; this occurs at frame 6N22. Point 62 on this B picture was selected as the initial point and its coordinates were computed by using the photo support data for this frame. Since the optical distance is about 3500 km, the circular standard error of location on the surface should be less than 17.4 km.

To tie Mariner 6 and 7 near-encounter points to the initial point 62, 306 observations of 66 points on these 16 pictures were combined in one solution. Point 62 was included among the fitting parameters although its corrections were constrained to be zero (by weighting the appropriate diagonal terms in the normal matrix). The internal accuracy of this solution is indicated by the weighted circular standard error of the recomputed residuals, which is 2.0 pixels or about 2.0 km at the nadir of 6N19. The standard errors of the computed areocentric coordinates range from 0.04° to 0.32° in latitude and from 0.04° to 0.47° in longitude, with an average value of 0.09° in latitude and longitude. The range of values for the standard errors is caused by scale and projection variations across the frames.

The next solution combines the Mariner 6 and 7 far-encounter frames with six common near-encounter points (2, 3, 50, 51, 52, and 79). Since points 2, 3, and 79 are well determined, in this solution their corrections are constrained to be zero. For points 50, 51, and 52, some freedom of adjustment is allowed because their coordinates are poorly determined in the near-encounter sequence. 374 observations of 31 points on 35 pictures were combined in this solution. The weighted circular standard error of recomputed residuals is 3.37 pixels, which corresponds to 50 km at the nadir and scale of frame 7F69. The range of internal standard errors of the computed areocentric coordinates is 0.22° to 1.01° in latitude and 0.22° to 2.04° in longitude, with an average value of 0.40° in latitude and 0.66° in longitude. In Table 6 the standard errors for each point in these far-encounter frames were determined with respect to point 62 by combining the average error of the six common points ($\langle\sigma\rangle_\phi$ = 0.18°, $\langle\sigma\rangle_\lambda$ = 0.22°) with the internal standard error of each point. The large variation in errors is caused

TABLE 7. Areocentric Coordinates of the Control Points

Control Point	Latitude ($\varphi°$)	σ_φ	W. Longitude ($\lambda°$)	σ_λ
1	18.91	0.37	134.64	0.42
2	−10.24	0.06	335.51	0.06
3	−9.64	0.06	337.18	0.05
4	−5.19	0.32	222.59	0.40
5	−13.42	0.05	350.55	0.05
6	1.80	0.12	7.70	0.08
7	−6.43	0.11	10.34	0.09
8	−7.33	0.11	10.26	0.09
9	−20.22	0.04	351.05	0.05
10	−4.66	0.09	6.52	0.07
11	0.20	0.10	11.05	0.07
12	−18.12	0.06	343.92	0.06
13	−16.04	0.05	349.15	0.05
14	−11.19	0.06	354.20	0.06
15	−19.54	0.11	26.81	0.16
16	−15.77	0.11	33.46	0.18
17	−24.21	0.09	339.08	0.08
18	−16.51	0.08	17.16	0.11
19	−12.93	0.08	15.72	0.10
20	−18.36	0.08	16.66	0.11
21	−14.76	0.11	31.58	0.17
22	−16.04	0.08	21.26	0.13
23	−27.62	0.07	346.06	0.08
24	−25.31	0.08	344.24	0.08
25	−60.30	0.36	24.57	0.67
26	−15.58	0.07	3.92	0.07
27	−13.72	0.07	2.61	0.07
28	−20.21	0.06	4.74	0.07
29	−19.63	0.06	3.55	0.07
30	−13.58	0.06	4.67	0.07
31	−6.11	0.07	358.96	0.06
32	−4.88	0.13	350.82	0.08
33	−4.33	0.09	356.30	0.07
34	−8.79	0.07	0.43	0.06
35	−4.94	0.08	2.51	0.06
36	−39.98	0.07	317.52	0.08
37	0.26	0.11	358.38	0.08
38	−4.09	0.08	0.90	0.06
39	−10.44	0.07	359.10	0.07
40	−60.53	0.36	6.58	0.56
41	−61.39	0.35	4.61	0.52
42	−60.75	0.37	14.74	0.56
43	−62.45	0.38	17.13	0.59
44	−63.67	0.41	33.67	0.81
45	−61.08	0.34	353.36	0.57
46	−59.34	0.36	358.71	0.87
47	−75.32	0.36	297.01	2.10
48	−63.59	0.35	344.60	0.58
49	−77.67	0.51	1.36	1.20
50	0.77	0.24	45.94	0.28
51	3.95	0.29	53.80	0.37
52	−1.35	0.32	59.19	0.46
53	−71.01	0.41	349.95	0.77
54	−65.63	0.37	349.22	0.61
55	−73.79	0.46	17.29	1.01
56	−15.90	0.05	351.07	0.05

TABLE 7. *(continued)*

Control Point	Latitude ($\varphi°$)	σ_Q	W. Longitude ($\lambda°$)	σ_λ
57	−73.06	0.45	25.08	1.11
58	−14.22	0.05	352.45	0.06
59	−12.69	0.05	349.59	0.05
60	−20.03	0.05	350.69	0.06
61	−16.77	0.05	349.60	0.05
62	−15.63	0.00	339.70	0.00
63	−19.65	0.04	340.72	0.05
64	−18.19	0.04	338.17	0.04
65	−12.18	0.05	339.41	0.05
66	−80.95	0.56	354.39	1.65
67	−74.82	0.43	333.61	1.18
68	−76.86	0.47	339.14	1.76
69	−30.27	0.07	345.34	0.08
70	−76.07	0.42	323.30	1.52
71	−76.60	0.35	306.33	1.39
72	−60.28	0.36	8.58	0.59
73	−60.80	0.49	90.62	0.77
74	−4.58	0.32	89.89	0.44
75	30.42	0.54	63.61	0.72
76	1.57	0.33	119.29	0.39
77	37.40	0.52	180.39	0.91
78	−60.48	0.53	151.03	0.68
79	−4.34	0.09	347.87	0.07
80	−45.66	0.07	317.72	0.09
81	−13.21	0.32	185.83	0.45
82	1.56	0.31	238.08	0.37
83	24.43	0.33	213.23	0.44
84	−10.74	0.28	320.26	0.31
85	21.85	0.31	295.35	0.36
86	−2.81	0.32	303.08	0.36
87	−39.83	0.32	237.45	0.45
88	−46.22	0.06	318.34	0.09
89	−43.13	0.07	315.55	0.08
90	−4.35	0.33	329.63	0.39
91	−38.68	0.08	316.36	0.08
92	−46.93	0.40	218.74	0.59
93	−60.84	0.45	237.99	0.80
94	−62.77	0.56	259.24	0.94
95	−61.49	0.68	301.44	0.97
96	−61.21	0.64	188.88	1.32
97	−60.96	0.52	181.68	1.32
98	−41.45	0.06	333.22	0.09
99	−37.17	0.08	328.93	0.09
100	−33.92	0.08	332.05	0.08
101	−40.79	0.06	332.14	0.09
102	−40.30	0.06	332.71	0.09
103	−60.53	0.65	52.75	1.40
104	−58.63	1.01	41.61	2.05
105	−6.92	0.28	271.26	0.33
106	−2.36	0.17	36.68	0.20
107	−9.32	0.14	32.41	0.18
108	−5.42	0.15	34.77	0.19
109	−7.41	0.16	42.82	0.22
110	−9.36	0.06	352.83	0.06
111	−11.21	0.05	351.09	0.05
112	−17.39	0.09	23.09	0.13

by convergence of longitudes at high latitudes as well as scale and projection effects.

The final solution ties the five Mariner 7 polar cap frames by means of 108 observations of 21 points. It has not been possible to find any point common to this strip and a far-encounter picture, so these were located by minimizing the sum of the squares of the residuals without any constraint on the [C] matrices. Thus the strip is internally consistent; however, it is not tied directly to the preliminary control net. The range of internal standard errors of the coordinates is 0.34° to 0.56° in latitude and 0.52° to 1.76° in longitude, with averages of 0.40° in latitude 0.98° in longitude.

An initial point (62) was used as a reference latitude and longitude in the computation of the preliminary control net. This is not the only way to obtain reference coordinates; in fact, the least-squares solution for best fit of the far-encounter pictures only will yield coordinates for all the points without further reference. Early attempts to obtain this form of solution indicated that minor changes in point measurements resulted in rather large longitude shifts of the entire net. No doubt this problem was due, at least in part, to the small number of measured points per picture. Useful points have been difficult to find on the far-encounter pictures. Only a few craters (such as point 4) can be identified on a large number of frames, so most of the chosen points are albedo markings (light or dark spots). Accurate measurements of the center of these spots are difficult to make and standard errors of over three pixels are not uncommon from multiple measurements of the same point (for reference, the nadir pixel size is about 5 km on 6F49 and 8 km on 6F43). Also, there is little confidence that the identical point is being measured on all pictures, as the shape of the spot changes from picture to picture.

This lack of precision of the far-encounter data led to the decision to use the initial point (62) to locate the near-encounter sequence. The near-encounter pictures suffer from minimum overlap and poorly calibrated cameras; however, their control points are usually the centers of well-defined craters so that multiple measurements of the same point always yield standard errors of less than one pixel, and errors of less than one-quarter pixel are not uncommon.

Further work is planned that will include increasing the number of points on the far-encounter pictures and the quality of their measurements. Also, a new improved calibration program, developed by R. B. Leighton, will be used to replace the GEOM 3 program. It is hoped that these improvements will permit meaningful solutions for planetary radii, independent estimates of longitudes (including point 62), and perhaps some suggestion for improvement of the spin axis.

Acknowledgments. Approximately a year before encounter, a Cartographic Working Group[1] was organized to investigate methods and techniques that would be useful in the establishment of a control net of Mars based on the expected Mariner pictures. The monthly meetings were valuable in designing data reduction procedures for television pictures; these included measurements, analytic and computer techniques, and cartographic portrayal. Many of the methods and ideas used in the current data-reduction program of the Mariner 6 and 7 pictures had been proposed and tested by members of the working group.

We would like to express our thanks to C. F. Martin, D. L. Meyers, and G. T. Stentz of ACIC for their help and advice in all phases of the data reduction problem, and to D. W. G. Arthur of the USGS for his helpful discussions and for suggesting the form of the observation equations, the approximate method for computing the partial derivatives, and the technique used for determining the corrections to the matrices. We are indebted to G. Hoover, B. Herman, and R. West of Caltech for carrying out the extensive measurements program; to J. van der Woude for photographic support of this program and the preparation of the figures; and to W. E. Kirhofer and J. K. Campbell of JPL for furnishing the trajectory data. We thank G. E. Danielson, Jr., S. A. Collins, and J. A. Dunne, JPL, for supplying us with the many special versions of pictures required for this work.

This research was partly supported by the National Aeronautics and Space Administration, at Rand by JPL Purchase Order GP-501936 and at ACIC by Contract Number NAW 12402. The opinions expressed herein are those of the authors

[1] Participants in the working group varied somewhat from meeting to meeting, but typically included S. E. Dwornik, W. H. Shirey (NASA Headquarters), R. A. Berg, D. L. Meyer, C. F. Martin (Aeronautical Chart and Information Center), J. C. Hammack, D. L. Light, J. B. Schreiter, J. M. Stephens (U.S. Army Topographic Command), D. W. G. Arthur (U.S. Geological Survey), R. B. Leighton (California Institute of Technology), J. K. Campbell, V. C. Clark, Jr., A. G. Herriman, W. E. Kirhofer (Jet Propulsion Laboratory), with M. E. Davies (The Rand Corporation) chairman.

and should not be construed as representing the opinions or policy of any agency of the U. S. Government.

REFERENCES

Adams, L., J. Cutts, J. Kent, C. Mahoney, P. Squyres, and S. Seng, *Mariner Mars 1969 Television Experiment Science Calibration Report*, pp. 3, 2–4, 47–65, *Jet Propul. Lab., 605–149*, Pasadena, Calif., Feb. 1, 1970.

Arthur, D. W. G., The computation of selenodetic coordinates using the librations, *Communications of the Lunar and Planetary Laboratory*, vol. 4, part 2, pp. 89–95, University of Arizona, Tucson, 1965.

Arthur, D. W. G., A new secondary selenodetic triangulation, *Communications of the Lunar and Planetary Laboratory*, vol. 7, part 5, pp. 303–306, University of Arizona, Tucson, 1968.

Berg, R. A., *ACIC Support of the Reduction of Mariner Mars 1969 (MM69) Television Photography*, pp. 175–177, Aeronautical Chart and Information Center, St. Louis, Mo., May 1970.

Brown, D. C., The simultaneous determination of the orientation and lens distortion of a photogrammetric camera, *RCA Data Reduct. Rep. 33*, 1956.

Campbell, J. K., *Mariner Mars 1969 Simulated TV Pictures (Final), Jet Propul. Lab., 605–237*, June 15, 1970.

de Vaucouleurs, G., The physical ephemeris of Mars, *Icarus, 3*(3), 236–247, 1964.

Leighton, R. B., N. H. Horowitz, B. C. Murray, R. P. Sharp, A. G. Herriman, A. T. Young, B. A. Smith, M. E. Davies, and C. B. Leovy, Mariner 6 television pictures: First report, *Science, 165*, 684–690, 1969*a*.

Leighton, R. B., N. H. Horowitz, B. C. Murray, R. P. Sharp, A. G. Herriman, A. T. Young, B.A. Smith, M. E. Davies, and C. B. Leovy, Mariner 7 television pictures: First report, *Science, 165*, 787–795, 1969*b*.

Leighton, R. B., N. H. Horowitz, B. C. Murray, R. P. Sharp, A. G. Herriman, A. T. Young, B. A. Smith, M. E. Davies, and C. B. Leovy, Mariner 6 and 7 television pictures: Preliminary analysis, *Science, 166*, 49–69, 1969.

Rindfleisch, T. C., J. A. Dunne, H. J. Frieden, W. D. Stromberg, and R. M. Ruiz, Image processing of the Mariner 6 and 7 pictures, *J. Geophys. Res., 76*, this issue, 1971.

(Received July 30, 1970;
revised September 16, 1970.)